# Relationship between structures, stress and seismicity in the Charlevoix seismic zone revealed by 3-D geomechanical models: Implications for the seismotectonics of continental interiors

A. F. Baird,[1] S. D. McKinnon,[1] and L. Godin[1]

Received 4 March 2010; revised 11 July 2010; accepted 3 August 2010; published 6 November 2010.

[1] The Charlevoix seismic zone in the St. Lawrence valley of Québec is the most active in eastern Canada. The structurally complex region comprises a series of subparallel steeply dipping Iapetan rift faults, superimposed by a 350 Ma meteorite impact structure, resulting in a heavily faulted volume. The elongate seismic zone runs through the crater parallel to the rift. Most large events localize outside the crater and are consistent with slip along the rift faults, whereas background seismicity primarily occurs within the volume of rock bounded by the rift faults within and beneath the crater. The interaction between rift and crater faults is explored using the three-dimensional stress analysis code FLAC3D. The rift faults are represented by frictional discontinuities, and the crater is represented by a bowl-shaped elastic volume of reduced modulus. Differential stresses are slowly built up from boundary displacements similar to tectonic loading. Results indicate that weakening the rift faults produces a stress increase in the region of the crater bounded by the faults. This causes a decrease in stability of optimally oriented faults and may explain the localization of low-level seismicity. Additionally, slip distribution along the rift faults shows that large events localize at the perimeter of the crater and produce focal mechanisms with P axes oblique to the applied stress field, consistent with historic large earthquakes. It is speculated that similar systematic rotation of focal mechanism P axes may be expected along other intraplate rift zones, raising a potential caveat for the use of focal mechanisms for stress estimation in continental interiors.

**Citation:** Baird, A. F., S. D. McKinnon, and L. Godin (2010), Relationship between structures, stress and seismicity in the Charlevoix seismic zone revealed by 3-D geomechanical models: Implications for the seismotectonics of continental interiors, *J. Geophys. Res.*, *115*, B11402, doi:10.1029/2010JB007521.

## 1. Introduction

[2] The Charlevoix seismic zone (CSZ) in the St. Lawrence valley of Québec is the most seismically active region in eastern Canada (Figure 1). It has been the site of several large historic events (five moment magnitude $M > 6$ events since 1663) [*Adams and Basham*, 1991] as well as continuous low-level activity. Like most intraplate earthquake zones, the cause of the focus of seismic activity is not well understood. On a broad scale, intraplate seismicity is often associated with preexisting weak structures such as ancient rift zones and aulacogens [e.g., *Sykes*, 1978]; however, small areas of intense activity are often attributed to local effects. The CSZ lies at the intersection of two potential sources of weakness; the Cambro-Ordovician St. Lawrence rift, which strikes NE-SW along the river, and the Charlevoix Impact structure, which is a large bowl shaped damage zone formed as a result of a meteorite impact ~300 Ma [*Rondot*, 1971].

[3] The relative importance of the two structures in the distribution of seismicity has been debated. *Leblanc et al.* [1973], noting several small events coinciding with the location of large past events and a meteorite crater, proposed that weakened crust caused by the impact could yield more easily to postglacial strain. Extensive microseismic monitoring further delineated the extent of the seismic zone, and revealed that there were in fact two clusters of seismicity running along the length of the St. Lawrence, which coincide with the interpreted location of rift faults [*Anglin*, 1984]. This information, combined with an absence of seismicity at other Canadian meteorite craters, led *Adams and Basham* [1991] to attribute the earthquakes to the reactivation of rift faults, possibly weakened by the crater. Improvements in hypocenter location and analysis of microseismicity focal mechanisms in the 1990s however, has revealed that much of the seismicity clusters are not occurring along planar structures, but appear to be located in fractured volumes of rock bounded by the major rift faults [*Lamontagne*, 1999]. Thus

[1]Department of Geological Sciences and Geological Engineering, Queen's University, Kingston, Ontario, Canada.


0148-0227/10/2010JB007521

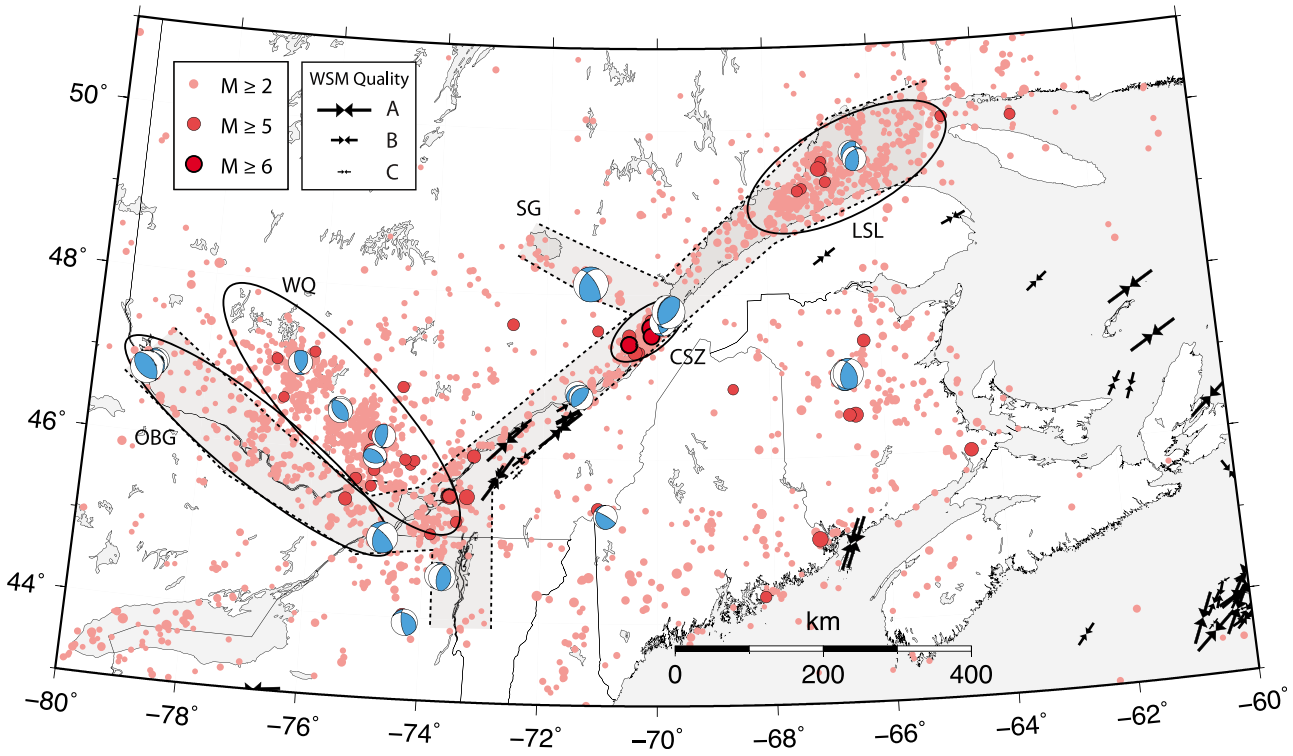


**Figure 1.** Seismicity and seismic zones in southeastern Canada. Background seismicity (Nuttli magnitude, $m_N$, ≥ 2 since 1985) from the Geological Survey of Canada, supplemented by large historic events (mostly moment magnitude, $M \geq 5$) since 1663 from *Lamontagne et al.* [2007]. Selected focal mechanisms of moderate to large earthquakes ($M \geq 4.3$) from the compilation of *Mazzotti and Townend* [2010]. Inverted black arrows indicate the orientation of $S_H$ inferred from borehole breakouts from the World Stress Map with quality ranking A (±15° uncertainty), B (±20°), or C (±25°) [*Heidbach et al.*, 2008]. Shaded grey area indicates the extent of Iapetan rifting [*Adams and Halchuk*, 2003]. Abbreviations: CSZ, Charlevoix Seismic zone; LSL, Lower St. Lawrence; OBG, Ottawa-Bonnechère graben; WQ, Western Québec seismic zone; SG, Saguenay graben.

both the impact structure and the rift faults appear to play an important role in the distribution of seismicity in the CSZ.

[4] While much has been published describing the seismicity in the CSZ, little work has been done to explain the mechanics behind the partitioning of seismicity. *Baird et al.* [2009], addressing this with simple 2-D stress models, showed that a series of parallel weak faults intersecting a "soft zone" can act as a stress conduit, channeling background stresses into the interior of the weak zone, which would otherwise simply flow around it. The models were used to illustrate this concept as a way to explain much of the background seismicity patterns observed in the CSZ. The models, however, had a number of limitations, primarily brought on by the restriction to two dimensions. The current study builds on the results of *Baird et al.* [2009] by extending the models to three dimensions in order to better represent the true 3-D architecture of the system. In addition to corroborating the results of the 2-D models, the 3-D models are used to explain the extension of earthquakes below the crater, address slip along the rift faults themselves, which appear to form the locus of the less frequent large events, and provide evidence for a misfit between focal mechanism P axes and the orientation of maximum horizontal compressive stress $S_H$.

## 2. Background

### 2.1. Geologic Setting

[5] The CSZ lies in a structurally complex setting created by a series of tectonic events spanning the last 1.1 Gyr (Figure 2a). The oldest tectonic episode recorded in the region consists of the 1100–990 Ma Grenville orogeny, which resulted from a series of exotic terranes accreting onto

**Figure 2.** (a) Seismicity and structural geology of the Charlevoix seismic zone. Pink and red circles represent earthquakes with Nuttli magnitudes ($m_N$) of less than 4.0 or greater than 4.0, respectively. Abbreviations: GNW, Gouffre northwest fault; SL, Saint-Laurent fault; CH, Charlevoix fault; SS, South Shore fault; LL, Logan's Line (Appalachian deformation front); $S_H$, Maximum horizontal compressive stress orientation. Lines B–B′ and C–C′ refer to cross sections in Figures 2b and 2c (earthquake data from the Geological Survey of Canada for the period 1985–2009). Cross sectional view of the Charlevoix seismic zone (b) across strike and (c) along strike of the St. Lawrence rift. Geological structure and crater boundary are based on the work of *Lamontagne* [1999] and *Rondot* [1994].

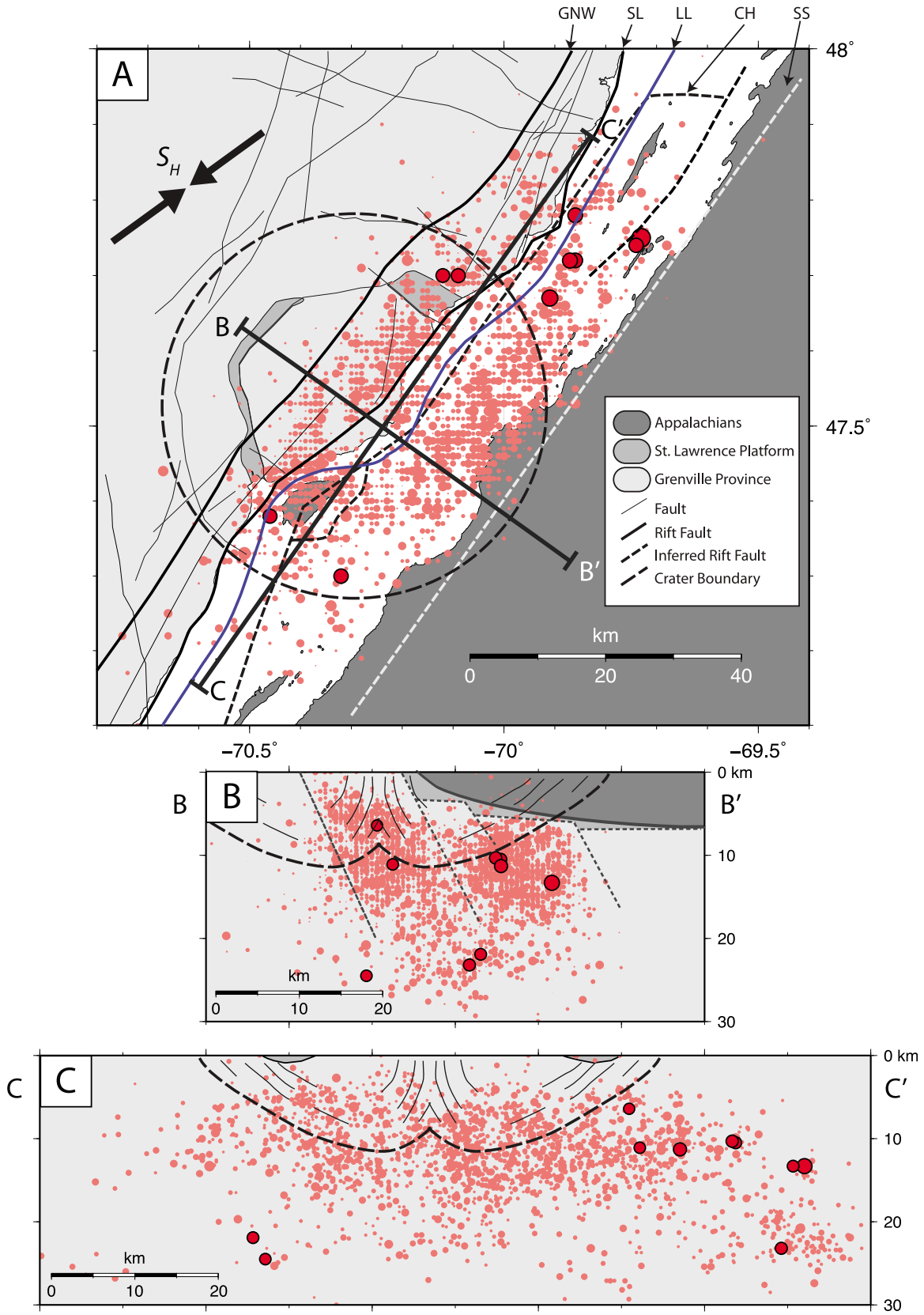
GNW
SL
LL
CH
SS
A
$S_H$
B
B′
C
C′
48°
47.5°
Appalachians
St. Lawrence Platform
Grenville Province
Fault
Rift Fault
Inferred Rift Fault
Crater Boundary
km
0
20
40
−70.5°
−70°
−69.5°
B
B
B′
0 km
10
20
30
km
0
10
20
C
C
C′
0 km
10
20
30
km
0
10
20

**Figure 2**

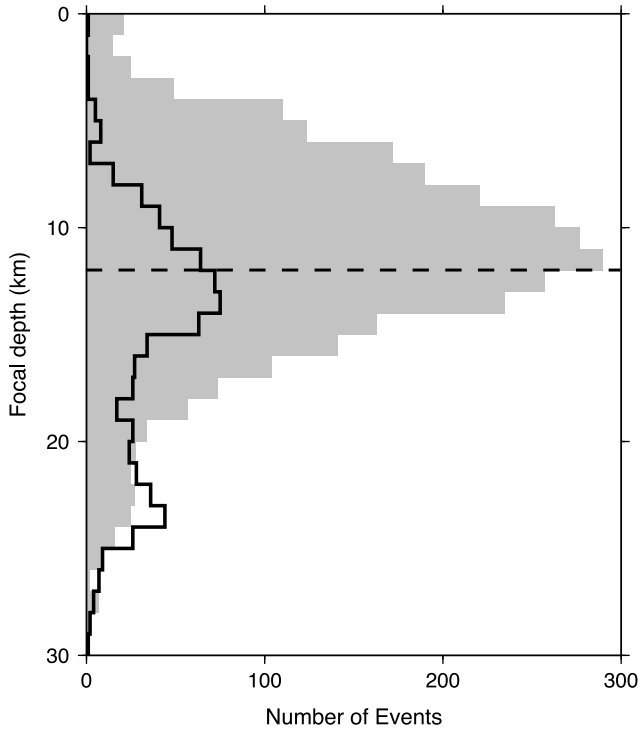


**Figure 3.** Earthquake depth distribution for events located within or directly below the crater (epicenters within 28 km from crater center, grey) and for the surrounding area (epicenters 28–70 km from crater center, black outline). Dashed line indicates approximate lower boundary of the crater. Data were compiled from the Geological Survey of Canada earthquake catalog.

the southeast margin of Laurentia [*Rivers*, 1997]. The upper amphibolite to granulite metamorphic facies rocks of the Grenville Province make up the core of this orogen and now form the basement of the Charlevoix area (Figure 2b). Following a period of erosion the area was subjected to a late Proterozoic to early Paleozoic rifting event associated with the breakup of the Rodinia supercontinent and the formation of the Iapetan Ocean [*Kumarapeli*, 1985]. A series of normal faults forming the St. Lawrence paleorift system represented the passive margin of the proto-North American continent onto which carbonate rocks of the St. Lawrence platform were deposited [*St-Julien and Hubert*, 1975]. The next major tectonic phase was associated with the closing of the Iapetan Ocean and the formation of the Appalachian orogen. Appalachian Nappes were thrust over the North American continent as far west as the St. Lawrence in the Charlevoix area. The deformation front, known as Logan's Line, runs through the CSZ [*Rondot*, 1994]. Following this, in the Devonian (~350 Ma) the region was subjected to a meteorite impact resulting in a large (~56 km diameter) crater [*Rondot*, 1971]. The last significant tectonic episode to effect the region was the normal sense reactivation of the Iapetan rift faults due to the opening of the Atlantic in the Mesozoic [*Lemieux et al.*, 2003].

[6] Since the Appalachian Nappes are confined to the upper few kilometers, and most of the seismicity is located in the deeper Grenville basement rocks, the most pertinent structural features are the rifted faults and the impact structure (Figure 2b). The NE-SW trending St. Lawrence rift is a half graben represented by a series of parallel normal faults steeply dipping to the SE, which extend into the Grenville basement [*Tremblay et al.*, 2003]. In the Charlevoix region these faults include the Gouffre northwest and St. Laurent faults that parallel the St. Lawrence river along its north shore, the Charlevoix fault, which lies under the river, and the South Shore fault, which does not outcrop on the surface but is inferred from gravity and magnetic data [*Lamontagne*, 1999] (Figures 2a and 2b).

[7] The Charlevoix impact structure forms a ~56 km diameter damaged zone exhibiting varied fault orientations. The faults include a polygonal ring graben system between 16 and 20 km from the center [*Rondot*, 1994] in which rocks of the St. Lawrence platform are locally preserved (Figure 2). In the interior portion of the crater the faults are more scattered in orientation [*Lemieux et al.*, 2003]. Faulting associated with the crater is estimated to extend to a depth of approximately 12 km [*Rondot*, 1994].

### 2.2. Seismicity

[8] The CSZ has been the locus of five earthquakes greater than $M$ 6 in recent history (in 1663, 1791, 1860, 1870, and 1925) [*Adams and Basham*, 1991]. The site is also host to an abundance of background seismicity. Over 200 events are recorded each year, most of which are lower than Nuttli magnitude ($m_N$) 3.0. Earthquakes occur almost entirely within the Grenville basement, with most activity between 7 and 15 km depth, but with some as deep at 30 km (Figure 2c).

[9] The spatial distribution of the background seismicity appears to be largely controlled by the St. Lawrence rift and the impact structure. The seismically active region spans approximately 30 by 85 km covering the area of overlap between the two structures and extending beyond the boundaries of the crater along the rift to the northeast (Figure 2a). A cross-sectional view of the seismicity across the strike of the rift reveals that earthquakes cluster into two distinct elongate zones, with the northwest cluster steeply dipping to the southeast (Figure 2b). The similarity in orientation of these clusters with the St. Lawrence rift faults led *Anglin* [1984] to conclude that most of the seismicity was related to reactivation of the faults. Improvements in hypocenter locations over the years, however, combined with evidence of varied slip planes from microseismic focal mechanisms suggest that much of the activity is not located on the major faults but within a fractured volume bounded by the rift faults [*Lamontagne*, 1999].

[10] Although the active region of the CSZ extends beyond the boundaries of the crater, most of the low-magnitude background activity occurs either within or beneath it (Figures 2c and 3). The large increase in shallow events within the crater area relative to the surrounding regions is strongly suggestive of its influence on the seismicity of the area. This is unusual, however, since most large impact structures found worldwide are seismically inactive [*Solomon and Duxbury*, 1987].

[11] While the impact structure appears to be strongly associated with low-level background seismicity, the opposite is true for larger events. As shown in Figure 2, all events larger than $m_N$ 4.0 (red circles) since 1985 have occurred outside the crater, with most clustering at the northeast end.

Additionally most large events over the last century have occurred to the northeast of the crater, including the 1925 $M$ 6.2 event and the 1979 $m_N$ 5.0 event [*Hasegawa and Wetmiller*, 1980; *Bent*, 1992]. Bearing in mind that the rupture surface of events of this magnitude are estimated to be on the order of several kilometers wide [*Johnston*, 1993], the localization of large events outside the crater as well as a common SE dipping nodal plane (Figure 4) suggest that the rift faults form the locus of these large events.

### 2.3. Stress Field

[12] The CSZ is located within the midplate stress province of eastern North America, which is dominated by NE to ENE oriented maximum horizontal compressive stress ($S_H$) [*Zoback and Zoback*, 1991]. Plate-driving forces from the Mid-Atlantic Ridge likely provide the greatest source of stress [*Richardson and Reding*, 1991; *Adams and Bell*, 1991; *Zoback and Zoback*, 1991]. The orientation of the stress field is inferred from a variety of data sources, which have been included in the World Stress Map database. In eastern Canada and the northeastern United States these are primarily borehole breakouts and earthquake focal mechanisms [*Heidbach et al.*, 2008].

[13] Borehole breakout data from the World Stress Map database for southeastern Canada are shown in Figure 1. These include a large number of measurements along the St. Lawrence river approximately 100–250 km southwest of the CSZ, between Québec City and Montréal, which are all consistently oriented NE-SW, subparallel to the river.

[14] Earthquake focal mechanisms provide another source of stress data where the P, B, and T axes are used to provide an estimate of the principal stress orientations [*Zoback*, 1992a]. However, P and T axes can potentially differ significantly from the actual stress orientations with the only strict constraint being that the orientation of the major principal stress must lie within the dilatational field of the focal mechanism [e.g., *McKenzie*, 1969]. Consequently it is current practice that all stress orientations inferred from individual focal mechanisms are given a quality ranking of no more than C (±25° uncertainty) regardless of how well the mechanism is constrained [*Barth et al.*, 2008]. Despite these problems, focal mechanisms do provide some constraint on the stress orientation and also contain useful information on the geometry of fault slip.

[15] A case study was carried out by *Zoback* [1992b], examining the focal mechanisms of 32 moderate earthquakes in eastern North America to determine whether slip was compatible with the regional stress field. A similar study by *Du et al.* [2003] supplemented the data with 16 more moderate events since 1990. Of the events examined, most were broadly compatible with the regional stress field, with NE-SW oriented P axes. However, there were a few notable exceptions, including four events located along the St. Lawrence river (two from the CSZ), which had P axes oriented NW-SE (Figure 1). *Zoback* [1992b] found that while the 1979 Charlevoix earthquake was geometrically possible in the inferred regional stress field, it was frictionally unlikely, requiring either very weak faults or superlithostatic pore pressure. Alternatively it was argued that it was related to a local stress perturbation, possibly due to the presence of a dense rift pillow beneath the St. Lawrence [*Zoback*, 1992b]. Similar models have been proposed to explain the earthquake concentration in the New Madrid seismic zone in the central United States, which is located within the Reelfoot rift [*Grana and Richardson*, 1996], and to explain an apparent stress rotation near the Amazonas rift in Brazil [*Zoback and Richardson*, 1996]. Published studies, however, are insufficient to support or refute the existence of a rift pillow beneath the St. Lawrence [*Du et al.*, 2003].These models also fail to account for the large number of borehole breakout data indicating rift parallel compression between Québec City and Montréal (Figure 1).

[16] One of the major shortcomings of these broad regional focal mechanism studies is the limited data sets used. All four of the anomalous events examined along the St. Lawrence were larger than $M$ 4. Examining a variety of focal mechanisms from the CSZ, however, reveals that while larger events ($m_N > 4$) typically have NW-SE oriented P axes, smaller events are considerably more varied (Figure 4). A formal stress inversion of 60 focal mechanisms carried out by *Mazzotti and Townend* [2010] yields a $S_H$ orientation of 086° for the whole of the CSZ, an approximately 30° clockwise rotation from $S_H$ inferred from borehole measurements. A more detailed analysis into spatial variations of stress within the CSZ, however, reveals two distinct estimates of $S_H$ orientation between events clustering northwest of the Saint-Laurent fault versus those from the southeast (Figure 4). A 47° apparent rotation exists between the two groups, with the NW cluster roughly parallel to the borehole data and the rift trend, and the SE cluster strongly oblique to it [*Mazzotti and Townend*, 2010].

[17] The significance of the large apparent rotation between the borehole and focal mechanism inferred $S_H$ orientations is not clear at this time. However, the variations in $S_H$ derived from microseismicity from within the CSZ suggest that it is a very localized effect and likely not due to a regional stress perturbation. Discussion of possible mechanisms causing the rotation is addressed later in this paper.

## 3. Numerical Approach

[18] *Baird et al.* [2009] used a 2-D stress analysis code to investigate the interaction between the rift faults and crater by locally altering the regional stress field and controlling the distribution of seismicity. In this paper we take a similar approach using the 3-D code FLAC3D (Fast Lagrangian Analysis of Continua) [*Itasca Consulting Group Inc.*, 2005]. FLAC3D uses finite difference techniques to compute stress and strain within discretized continuum blocks while permitting the inclusion of a small number of discontinuities to represent discrete faults.

[19] The main reason for using a 3-D code is to better represent the true architecture of the system and to allow oblique slip displacements along modeled faults, which were previously restricted to strike-slip. For simplicity we limit the structures included to only those features which play an important role in the distribution of seismicity, namely, the rift faults and the impact crater (Figure 5). The rift faults are represented as a series of three parallel frictional discontinuities striking at N035° and steeply dipping to the southeast. Due to difficulty in including curved interfaces to model listric faults, the models are tested with fault dips of 60° and 70°. The faults roughly correspond to the Gouffre northwest, Saint-Laurent and South Shore faults, which

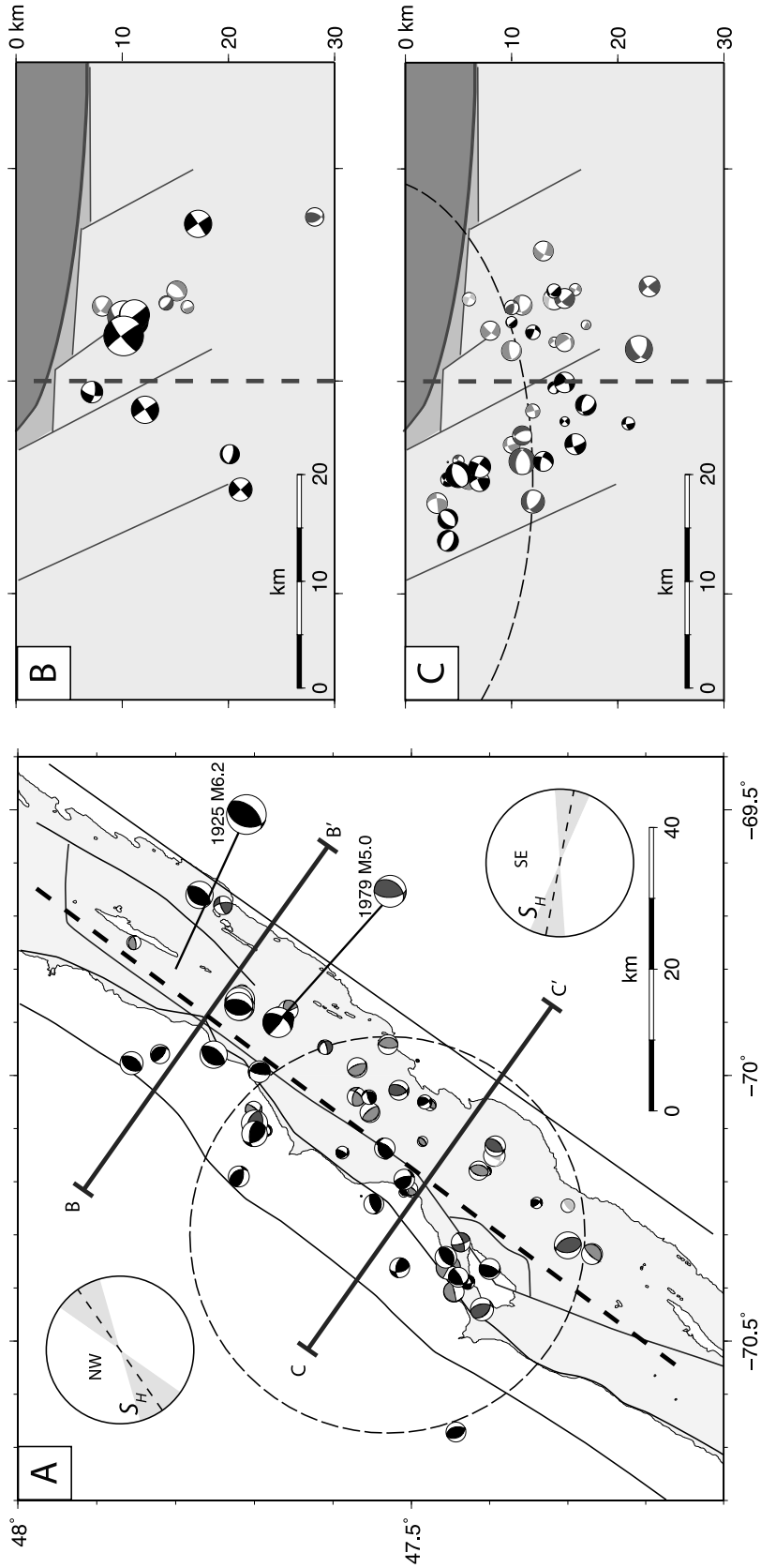


**Figure 4.** (a) Earthquake focal mechanisms from the Charlevoix seismic zone. Mechanisms are scaled by magnitude. Black, dark grey, and light grey mechanisms refer to quality rankings of A, B, and C, respectively. The two largest events ($M$6.2 1925 event and $m_N$ 5.0 1979 event) are indicated. Circles with dashed lines and grey angular sectors indicate the average and 90% confidence regions of the maximum horizontal compressive stress direction in the NW and SE clusters of seismicity from the stress inversion of *Mazzotti and Townend* [2010]. (b) Cross section showing mechanisms northeast of the crater. (c) Cross section showing mechanisms within or below the crater. Thick dashed line indicates the separation of the NW and SE clusters of seismicity used in the analysis.

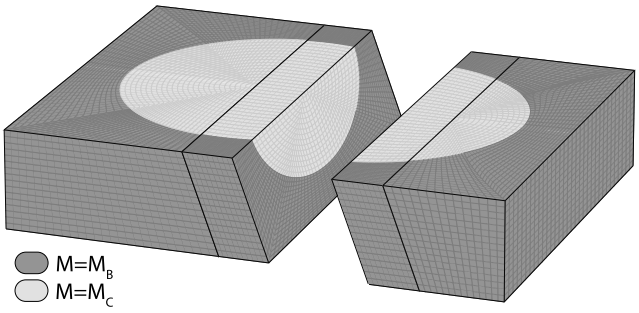


**Figure 5.** Internal geometry of the model. The crater is represented as an ellipsoid with a horizontal radius of 30 km and depth of 15 km at its center. Rift faults strike at 35° and are steeply dipping to the SE. Shading indicates variations of the elastic moduli ($M$) in the model between the background rock ($M_B$) and the weakened crater rock ($M_C$).

appear to form the main boundaries of the seismicity (Figure 2). The Impact structure is represented in the models as the lower half of an oblate spheroid, with a 30 km radius at the surface and extending to a depth of 15 km below the center. Rather than represent the complex faulted volume with explicit faults, the damaged volume is simulated by using a continuum of lowered elastic modulus following the well established concept of an equivalent continuum for fractured rock [e.g., *Fossum*, 1985].

### 3.1. Initial and Boundary Conditions

[20] An elastic continuum constitutive model is chosen to represent the crust in which density, bulk, and shear moduli must be prescribed. Density is assumed to be 2700 kg $m^{-3}$, typical of upper crustal rock. The background moduli for the region outside the crater (both bulk and shear, hereby denoted collectively as $M_B$) is derived from P and S wave velocity models for the Saguenay region to the north of the CSZ [*Somerville et al.*, 1990]. The variation of $M_B$ with depth is shown in Figure 6a. Within the crater, the elastic modulus values (denoted $M_C$) are lowered to simulate the damaged zone. Since the equivalent modulus is not known it was tested at 1/4 and 1/2 the value of the surrounding rock ($M_B$).

[21] Eastern Canada is characterized by a triaxial thrust regime state of stress (i.e., $S_H > S_h > S_V$) [*Adams and Bell*, 1991]. However, rather than initializing a differential stress in the models, a simple lithostatic stress field is initialized, and the horizontal compressive stress is then slowly increased through boundary displacements. This procedure ensures compatibility between the stresses and fault displacement. Since it is assumed that the largest contribution to stress in the region is from far-field tectonic sources, boundary displacements are applied in the direction of tectonic loading over a series of computational time steps. The stress field is slowly built up until the differential stress at a depth of 10 km is approximately 200 MPa (Figure 6b), which is of the same order of estimates of stress differences at that depth [e.g., *Hasegawa et al.*, 1985; *Zoback et al.*, 1993; *Lamontagne and Ranalli*, 1996].

### 3.2. Processing Technique

[22] The main purpose of the modeling is to understand the partitioning and distribution of seismicity. For this, we distinguish two classes of earthquakes: (1) earthquakes that occur off the main rift faults, on fractures and minor faults that are not explicitly modeled and (2) earthquakes that nucleate

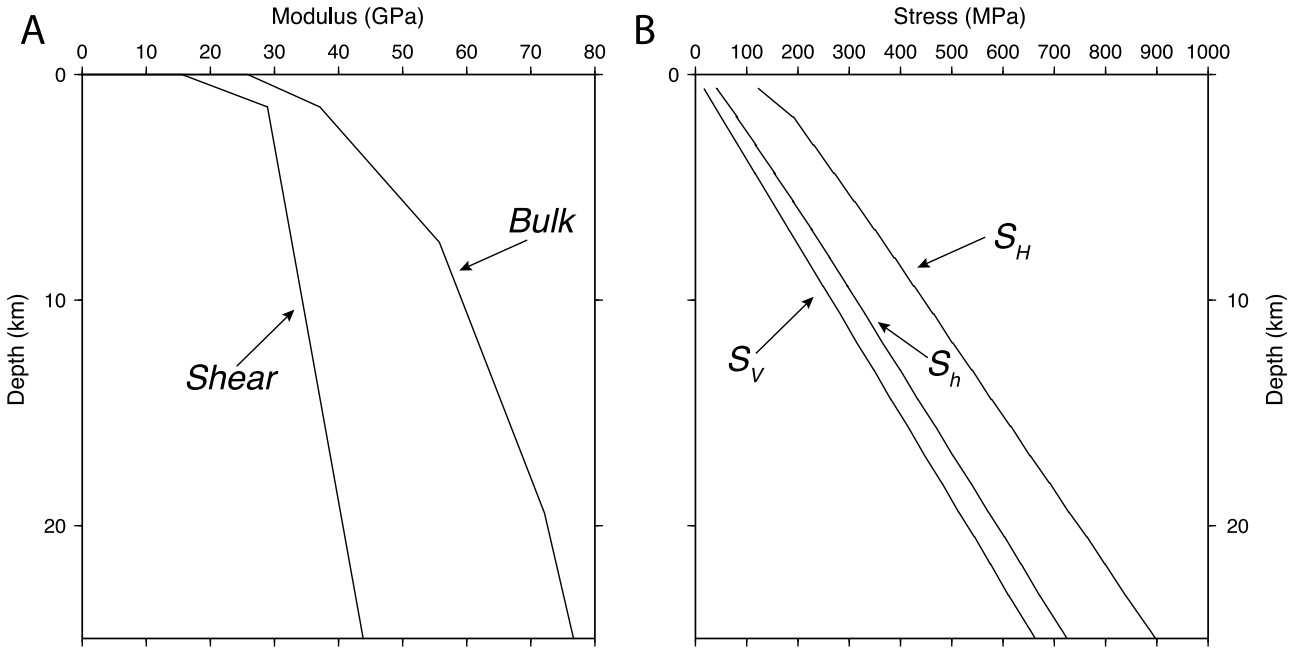


**Figure 6.** (a) Variation of bulk and shear modulus with depth at a region outside of the impact structure, as computed from the 1-D velocity model in the Saguenay region of *Somerville et al.* [1990]. (b) Final stress profile in region outside on the crater resulting from boundary displacements. $S_H$, $S_h$, and $S_V$ refer to the maximum horizontal, minimum horizontal, and vertical stresses, respectively.

along the major rift faults, which are explicitly included. We use different techniques to interpret the two classes of events.

#### 3.2.1. Earthquakes off the Rift Faults

[23] Events located away from the rift faults constitute the bulk of the low-level background seismicity that is observed in the CSZ, which are interpreted to cluster within fractured volumes bounded by the rift faults. Because the faults associated with these events are not explicitly included in the models, their stability must be inferred using alternative means. A useful parameter for inferring fault stability is differential stress ($\sigma_D$) which is proportional to maximum shear stress. Differential stress is defined as the difference in magnitude between the major and minor principal stresses:

$$\sigma_D = \sigma_1 - \sigma_3 \quad (1)$$

The presence of a high differential stress alone, however, does not necessarily lead to seismic activity. Other factors, such as confining pressure and the availability of optimally oriented fractures also play an important role. However, within a homogeneous randomly fractured rock mass an *increase* in differential stress would be expected to produce an increased incidence of seismicity. If there is no preferred fault orientation then stress release would be expected to be distributed over a variety of small faults rather than a large event on a single fault.

[24] For the Charlevoix model analysis, a control model is first developed that acts as a point of comparison for other models. Most large impact structures are seismically inactive [*Solomon and Duxbury*, 1987], and much of the background seismicity within the crater is thought to be the result of interaction with the rift faults. Consequently a suitable control model is one in which the rift faults are omitted and only the impact structure is modeled. Further models which incorporate weak rift faults can then be compared directly to the control model, which is assumed to be aseismic. For the analysis we define a new parameter $\Delta\sigma_D$:

$$\Delta\sigma_D = \frac{\sigma_{Dmodel} - \sigma_{Dcontrol}}{\sigma_{Dcontrol}} \quad (2)$$

where $\sigma_{Dmodel}$ and $\sigma_{Dcontrol}$ indicate the differential stress magnitude within a test model and the control model, respectively, for a common discretized zone. A positive value of $\Delta\sigma_D$ indicates regions which have had an increase in differential stress relative to the assumed aseismic control model, and thus an increase in the potential for earthquakes to occur. Conversely, a negative value of $\Delta\sigma_D$ would suggest a reduction in seismicity.

#### 3.3.2. Earthquakes on the Rift Faults

[25] Unlike the faults of the impact structure, the regional-scale rift faults are explicitly included in the models as discontinuities that are assigned Mohr-Coulomb frictional strength parameters. Fault stability can therefore be inferred simply by monitoring slip activity as the background differential stress is built up through boundary displacements. The build up of the stress in the model is done over 10,000 computational time steps (not linked to true time). To monitor temporal changes in slip activity a 100 step interval is arbitrarily chosen to represent a "small" amount of time. Relative slip displacement accumulated over the interval is then calculated for each fault grid point and plotted as a vector field indicating both magnitude and direction of slip of the hanging wall relative to a stable footwall. By viewing these vector fields as a time sequence, temporal variations in slip activity on the rift faults and their relationship to along-strike structural variations can be observed.

## 4. Results

### 4.1. Seismicity off the Rift Faults

[26] To analyze the stress models for seismicity off the main faults, the data are processed to calculate the change in differential stress ($\Delta\sigma_D$) caused by weak rift faults as defined in equation (2). Using this definition, positive values are expected to indicate regions where seismicity is promoted, particularly in areas where preexisting faults and fractures occur, such as in the interior of the crater. Figure 7 shows a series of sectional contour plots of this value, showing its 3-D distribution through a model with $M_C = 1/4 M_B$, weak rift faults with a friction angle of 5°, and an applied regional orientation of $S_H$ of N050° as inferred from borehole measurements [*Heidbach et al.*, 2008].

[27] At the shallower levels within the depth range of the crater (5 km and 10 km, Figure 7a), there is a clear increase in differential stress in the region of the crater bounded by the rift faults, which corresponds to the general pattern of background seismicity observed in the CSZ (Figure 2a). At deeper levels (15 km and 20 km) a similar pattern exists, although not as prominent as at shallow depths. Cross-sectional views, both across and along strike (Figures 7b–7d) show a pattern of increased stress concentrations between the rift faults, both within and beneath the crater, which match the general 3-D pattern of seismicity observed in the CSZ (Figure 2).

[28] To understand the reason for these stress concentrations, the effect of the relevant structures on the pattern of regional stresses must be examined. When the crater is considered on its own, without the influence of the rift, the trajectories of the major principal stress tends to flow around the structure (Figure 8a). This leaves the mechanically weaker material in the interior of the crater at a lower state of differential stress, thus diminishing the probability of earthquakes. When weak rift faults are also included in the model (Figure 8b), the largest effect is a local rotation of $S_H$ such that it becomes more parallel to the faults. While the effect of the reorientation is subtle (<15° rotation), it does disrupt the pattern of stress around the crater such that higher concentrations of differential stress form in the interior of the crater between the rift faults. In cross section the major principal axis of the stress field also flows beneath the crater, thus resulting in a higher differential stresses in this area as well (Figure 8c).

[29] The general pattern of stress partitioning is very similar to the main findings from *Baird et al.* [2009]. However, the 3-D models reveal some additional details observed in the CSZ that were not found in the 2-D models. One of the notable details of the seismicity distribution is an extension of the active zone along the rift to the northeast of the crater, while there is minimal background seismicity to the southwest (Figure 2). A similar pattern of increased differential stress to the northeast of the crater is observed in the model, most clearly at the 10 and 15 km depth sections (Figure 7a)

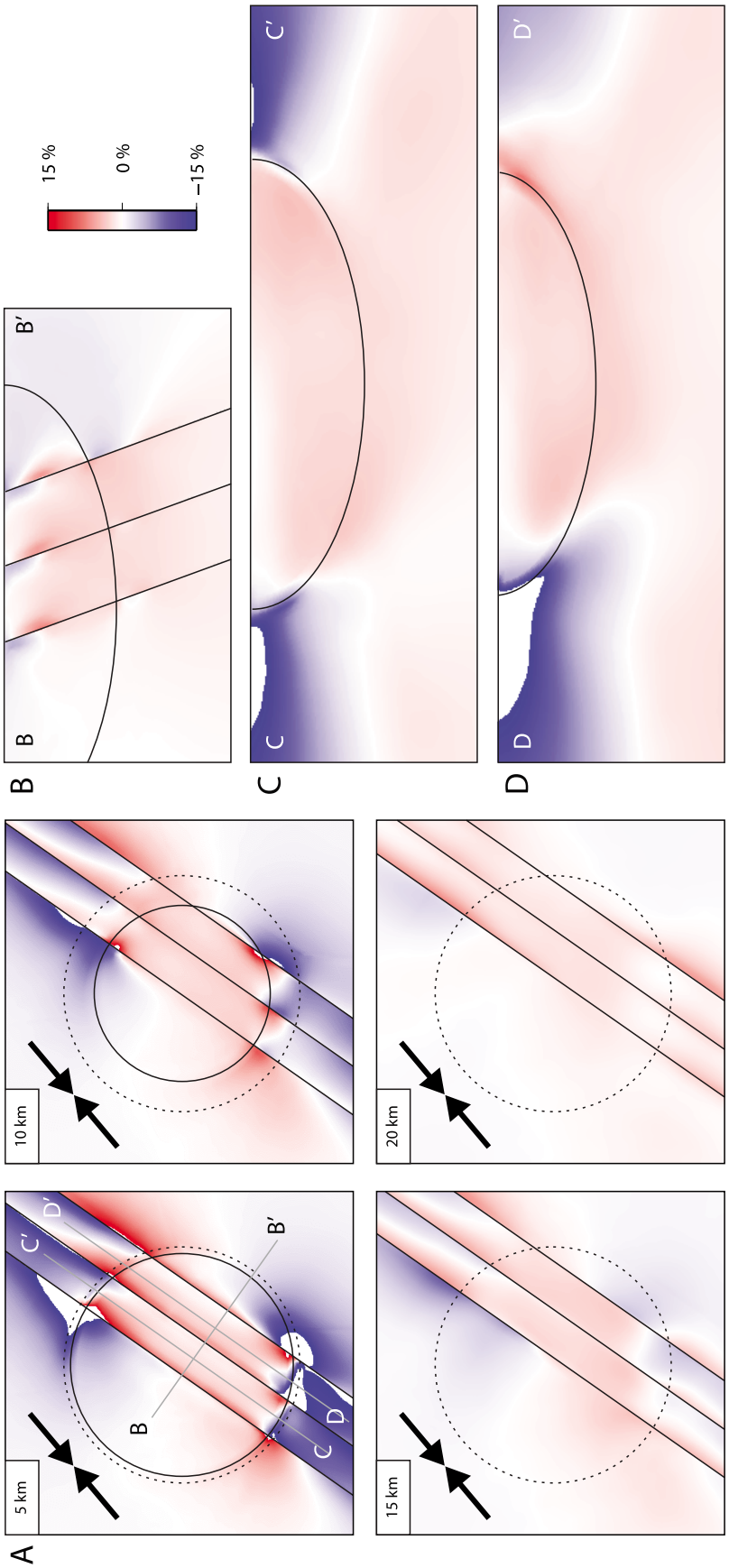


**Figure 7.** Sectional contour plots showing changes in differential stress relative to the control model using equation (2) for a model with $M_C = 1/4M_B$, a fault friction angle of 5°, and an applied regional $S_H$ orientation of 050°. (a) A series of horizontal depth sections. (b) A cross section through the center of the crater oriented perpendicular to the rift strike. (c and d) Cross sections parallel to rift strike, located between the northern and central fault (Figure 7c), and between the central and southern fault (Figure 7d).

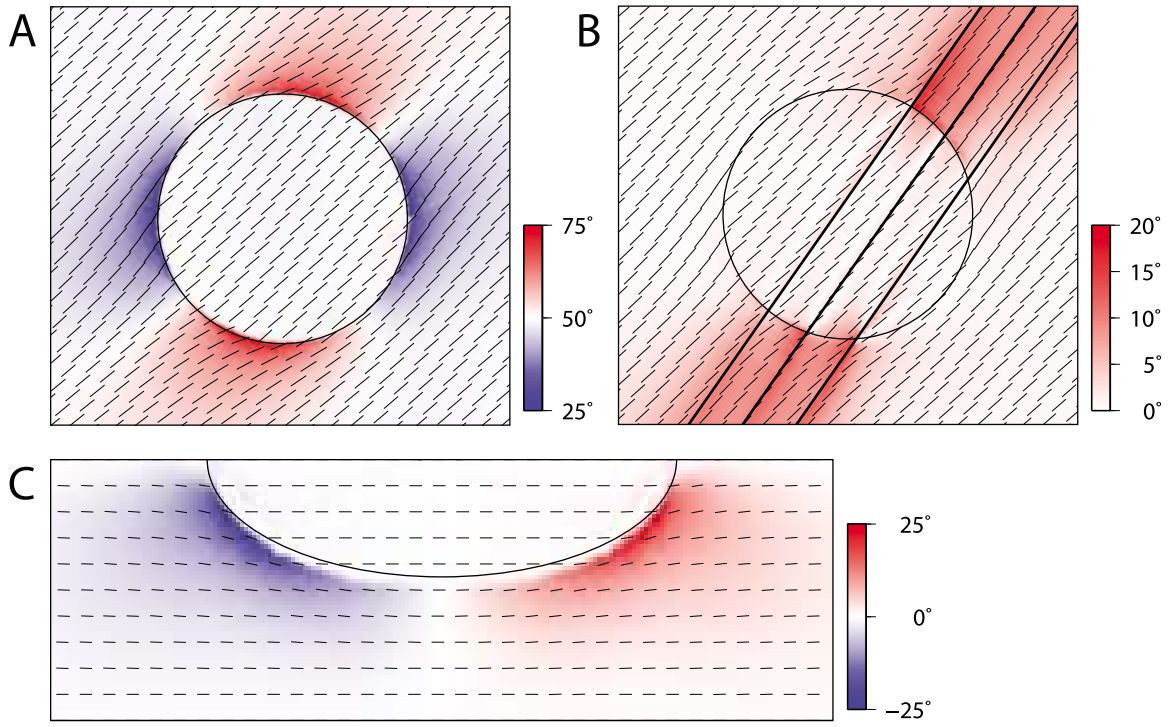


**Figure 8.** (a) $S_H$ orientation for stress applied to a crater with modulus 1/4 of the background at a depth of 5 km. Applied loading at 50°. (b) Same model as Figure 8a but with weak (5°) frictional faults included; contour plot indicates amount of rotation of $S_H$ relative to locked fault model shown in Figure 8a. (c) NW-SE vertical cross section, showing the deflection of $\sigma_1$ orientation beneath the crater.

and also in the cross sections along fault strike (Figure 7c). This effect is mainly a consequence of the asymmetry imposed on the system by the inclination of the applied stress field orientation relative to the rift fault orientation. This is illustrated in Figure 9 where the differential stress changes are plotted for models with applied loading at N045°, N055°, and N065°(equal to a 10°, 20° and 30° clockwise rotation from the strike of the rift). When the applied stress is at low angles to the rift, the region of increased differential stress extends out of the crater the most, however, the magnitude of this increase is low. At higher angles the extension out of the crater is reduced, but stress concentration inside the crater increases. An applied stress orientation of N050° as shown in Figure 7 forms a pattern which best matches the observed seismicity patterns, and is consistent with the inferred orientation of $S_H$ from borehole breakout measurements [*Heidbach et al.*, 2008].

### 4.2. Seismicity on the Rift Faults

[30] To analyze seismicity localized on the rift faults, the slip activity is monitored as stresses are progressively built up through boundary displacements. While this is not strictly equivalent to the buildup of tectonic stresses, it can be used to make some inferences of the relative stability of different portions of the faults. The behavior is best observed by viewing the animations provided in the auxiliary material.[1]

[1]Auxiliary materials are available in the HTML. doi:10.1029/2010JB007521.

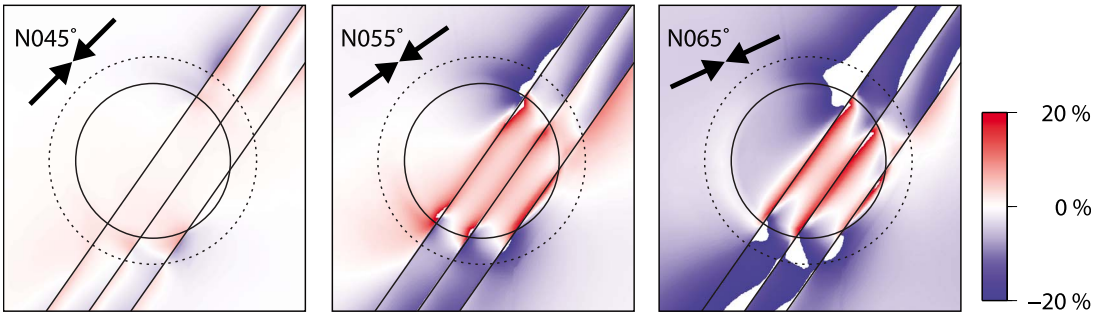


**Figure 9.** Contour plots of change in differential stress, showing the effect of varying the applied stress orientation.

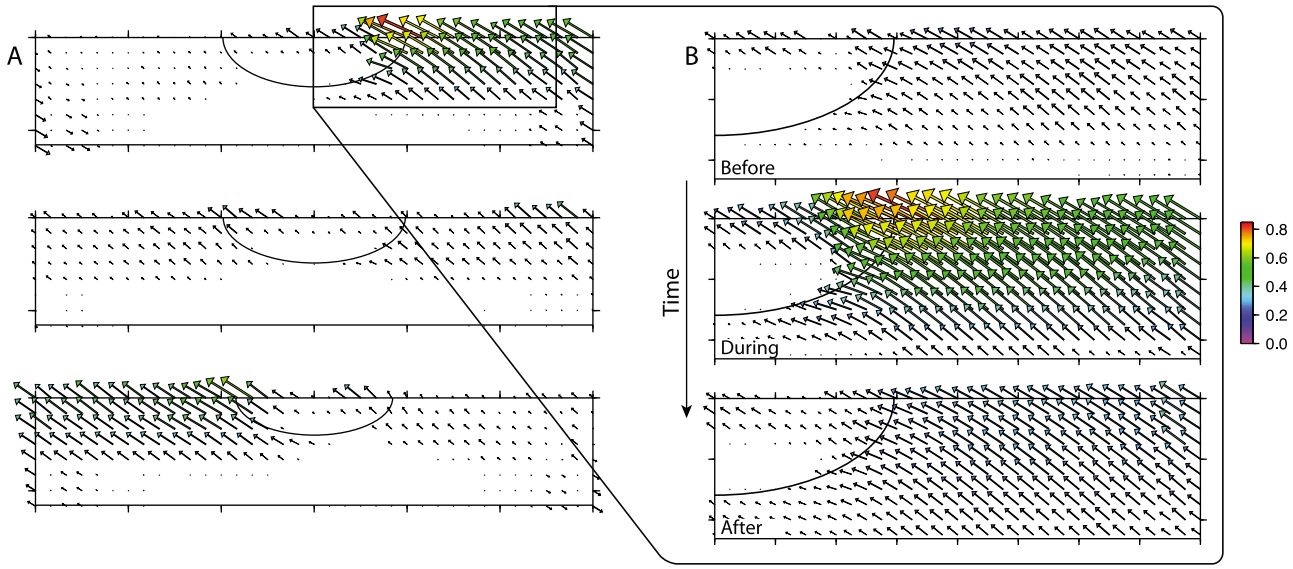


**Figure 10.** Vector plot showing relative shear displacement of the hanging wall of the rift faults. (a) The (top) northern, (middle) central, and (bottom) southern faults during one of the pulses of activity just outside the crater. (b) A close-up along the northeastern portion of the north rift fault before, during, and after a pulse event. Animations of the behavior can be found in the auxiliary material.

Figure 10 shows a vector field of the hanging wall shear displacement relative to a stable footwall for all three faults over a small time interval during the progressive boundary displacement (Figure 10a) and a closeup of the northern fault at the northeastern side of the crater before (Figure 10b, top), during (Figure 10b, middle) and after (Figure 10b, bottom) the activity shown in Figure 10a. At early times the stress field is effectively lithostatic and there is little motion along the faults. As differential stress is built up, the induced strain begins to be accommodated by fault slip, with most initial activity localized near the surface and then gradually migrating deeper. Inside the crater the amount of rift fault slip is noticeably lower than the activity outside. The focus of slip activity outside the crater migrates over time, showing a cyclical pattern where activity builds up on the northeast before decreasing to a background level and then increasing to the southwest of the crater. The maximum slip magnitude during these pulses of activity occurs just outside the perimeter of the crater (Figures 10a and 10b, middle).

[31] The slip partitioning along the rift faults appears to be largely the consequence of the modulus contrast between the crater and the surrounding rock. The rift faults represent a large-scale regional weak zone within a relatively strong crust. As a consequence of this, much of the far-field strain is accommodated by concentrated deformation along the rift. Along most of its extent the rift is surrounded by relatively stiff rocks, favoring slip along the discrete bounding faults. Where the rift passes through the crater there is a noticeable decrease in slip activity along the faults, and there is a corresponding increase of stress within the crater as a result of its interaction with the weak rift faults (Figure 7). This suggests that the decrease of fault slip is simply due to the transition from strain accommodation by discrete fault slip along the rift boundary faults to accommodation by bulk deformation where the rift passes through the damaged impact zone. The periodic large slip activity just outside the crater boundaries appears to be caused by the build up of shear stress on these faults due to the flow of stress around the crater (Figure 8).

### 4.3. Stress and Focal Mechanisms

[32] Perhaps the most puzzling aspect of the CSZ is the apparent inconsistencies in the inferred orientation of stress. Focal mechanism based stress inversions suggest that stress is oriented parallel to the rift in the NW cluster of events, but strongly oblique to the rift in the SE cluster (Figure 4) [*Mazzotti and Townend*, 2010]. Most available stress information is derived from focal mechanisms of events from within the seismic zone, for comparison purposes the modeled principal stress orientations from the approximate dimensions of the seismic zone are plotted in Figure 11a. It shows stress orientations from all grid points between the rift faults for depths shallower than 15 km between the southwest boundary of the crater, to 30 km past the northeast boundary of the crater (Figure 11b). Figure 11 shows an orientation of $S_H$ very similar to the applied loading directions. This matches the inferred $S_H$ orientation from the NW cluster of events, but it is inconsistent with the SE cluster, which shows a strong (~45°) clockwise rotation (Figure 4) [*Mazzotti and Townend*, 2010].

[33] Focal mechanism parameters for events on the rift faults in the model are computed using the fault geometry and slip vector data. Figure 11c shows a contour plot of the modeled P, T and B axes in a lower hemisphere projection. The most notable characteristic of this is the large (~35°) clockwise rotation of the P axis orientation relative to the direction of loading. The mechanism is similar in style to that of the large earthquakes observed in the CSZ, although the natural events typically have a larger thrust component than in the model. Figure 11d shows the resulting average mechanism if the fault dip is lowered to 60°. This results in further rotation of the P axis as well as a larger thrust component, providing a better match to the focal mechanisms of the

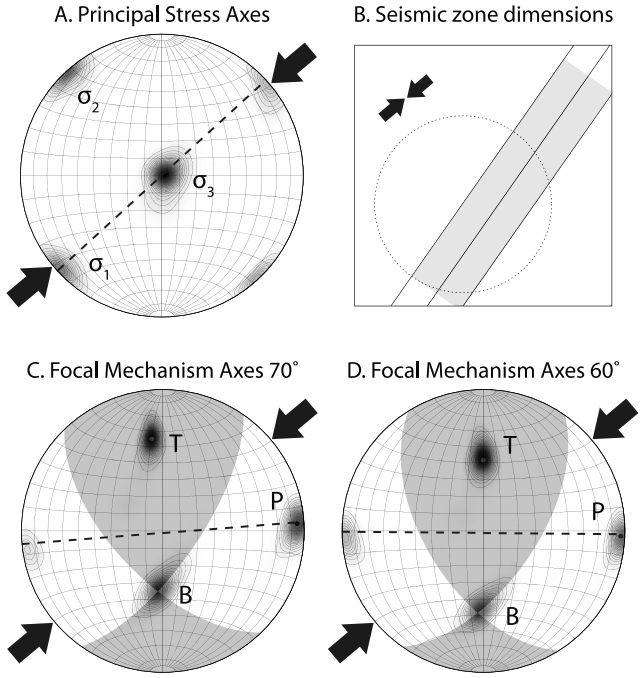


**Figure 11.** (a) Lower hemisphere stereonet contour plot of the principal stress orientations computed in the model within the upper 15 km of the region defined in Figure 11b. (b) Seismic zone dimensions. (c) The P, T, and B focal mechanism axes calculated using rift-fault slip vectors, with overlaid best fit focal mechanism solution for rift faults dipping at 70°. (d) Best fit focal mechanism for faults dipping at 60°. Large black arrows indicate the direction of loading applied to the model.

observed large events. It is likely that some variation of fault dip with depth (i.e., listric faults) could account for some variability in the observed style of mechanisms.

## 5. Discussion

[34] The models are able to reproduce many of the observed seismicity characteristics of the CSZ. The region of increased differential stress between the rift faults in the models shows a remarkably similar pattern to the observed background seismicity (Figure 7), including details such as the extension of the seismicity to the NE of the crater, which only occurs when the applied boundary conditions are close the regional orientation of $S_H$ as inferred by borehole data. The comparatively soft impact crater is shown to influence the stability of the rift faults intersecting it as it responds to regional strain from far-field boundary displacements (Figure 8). Rift fault slip is significantly reduced within the crater, where strain accommodation due to bulk deformation predominates (Figure 10). However, slip is locally promoted just outside the boundaries of the crater (Figure 10b); this corresponds spatially to the regions of large events observed in the CSZ (Figure 2). Additionally, the sense of slip along the faults implies a significantly rotated P axis compared to the applied regional stress (Figures 11c and 11d), which is similar in style to the focal mechanisms of large events at the CSZ (Figure 4).

[35] Although the models do address the apparent stress field rotation observed when considering only large events, they do not adequately explain the difference in $S_H$ orientation between the two rift parallel clusters of seismicity (Figure 4)[*Mazzotti and Townend*, 2010]. These stress orientations were calculated by a formal stress inversion technique using both large and small events. The difference between the model results and observations may be partially explained by considering the implications of some of the structural simplifications made in the model. The three large rift faults are the only true failure planes included in the models. All other material is represented by an isotropic continuum. The impact crater in reality is a complex faulted structure, which is simulated by representing the damaged zone as a continuum with reduced elastic properties. However, in doing so, much of the complexity is removed. The reduced elastic modulus representation is likely most valid in the central portion of the crater, which is characterized by a wide scattering of fracture orientations [*Lemieux et al.*, 2003]. In the outer portion of the crater, fault geometry is dominated by a ring graben structure, such that the prominent fault orientation is roughly parallel to the boundary [*Rondot*, 1994]. Mechanisms from the NW cluster yielded a $S_H$ orientation roughly parallel to the regional field (Figure 4). This is encouraging, as this cluster runs through the center of the crater, where the isotropic representation is likely more valid given the scattered orientation of fractures. The SE cluster, however, yielded a $S_H$ orientation strongly oblique to the rift, similar to the P axis orientation from large events [*Mazzotti and Townend*, 2010]. It is notable that this cluster occurs near the southeast boundary of the crater, where crater faults are likely to be preferentially oriented NE-SW similar to the rift faults. Perhaps more importantly, a large number of the focal mechanisms in this cluster extend beneath the lower boundary of the crater, into the rifted crust below (Figure 4c). In the models the rift is represented as three discrete faults, with no structure in the rocks between them. In reality these rocks likely exhibit minor faulting in a similar style to the regional faults, and thus have a prominent NE-SW orientation. The rifted block beneath the crater is still affected by a differential stress concentration due to the stress deflection beneath the crater; however, by analogy with the larger events, much of the minor event focal mechanisms in this area would be expected to reflect the local structure.

[36] One troubling requirement of the models is that the regional rift faults must be very weak, as they are poorly oriented for reactivation in the regional stress field. This weakness can be due to an unusually low frictional strength (as was used in the model), a very large pore fluid pressure, or by some combination of the two. While this is unusual it has been proposed as a possible explanation for the large thrust events in the CSZ [e.g., *Zoback*, 1992b; *Du et al.*, 2003]. *Lamontagne* [1999] proposed a model for the CSZ in which the rift faults could act as a conduit for fluids under pressure, causing an inherent weakness. Regardless of the source of fault weakness, its effect in the models leads to the formation of patterns of stress and seismicity compatible with observations.

## 6. Implications

[37] The suggestion that the St. Lawrence rift faults are inherently weak has broad implications for seismicity of the

St. Lawrence as a whole. While monitoring slip along the modeled faults (Figure 10), it is noted that outside of the crater zone, slip is on average evenly distributed along the rift, with the exception of somewhat increased pulses of slip just outside the crater. At any one time, however, only small segments of the faults are active. Based on this model behavior it can be speculated that slip activity in the St. Lawrence may migrate along strike over time, in which case seismic risk in currently quiescent areas of the rift valley may be underestimated. Seismic hazard maps based on historical seismicity often contain "bull's-eyes" of high hazard around areas with recent large earthquakes [*Stein*, 2007]. This may, however, be an artifact of the relatively brief seismic record. To account for the possible temporal migration along regional structures it may be beneficial to employ a more robust approach to hazard estimation using both historic seismicity and recognized regional structures that account for increased estimates between active seismic zones. Such an approach is currently used for hazard maps by the Geological Survey of Canada [*Adams and Atkinson*, 2003].

[38] The models also helps to clarify the unusually large range of focal mechanism patterns observed in the CSZ. In particular, the models highlight a possible scale dependence between large and small events, where moderate and large events are more influenced by regional structural trends than their smaller counterparts. This has broad implications for interpreting focal mechanisms at regional scales, particularly in intraplate settings. The models indicate that while stress tensors show little deviation from the applied orientation of $S_H$, focal mechanisms computed from slip along the weak rift faults produce a P axis at high angles to the applied stress (Figure 11). Restricting focal mechanisms to only those that occur along the rift faults would therefore result in a misleading estimate of $S_H$ orientation. It is argued that by restricting their data set to only moderate and large earthquakes, the regional focal mechanism studies of *Zoback* [1992b] and *Du et al.* [2003] introduced a structural bias to events occurring along larger-scale faults, resulting in a substantial apparent stress rotation along the St. Lawrence river (~60–90°, Figure 1). Studies that incorporate smaller magnitude focal mechanisms [e.g., *Adams and Bell*, 1991; *Mazzotti and Townend*, 2010] include events that occur on more variably oriented minor faults. These generally result in average stress orientation estimates closer to the regional field as measured from borehole data, but still with a significant clockwise rotation (~30–45°). The detailed stress inversion results from within the CSZ of *Mazzotti and Townend* [2010] showed that mechanisms from the NW cluster of events yielded a $S_H$ approximately parallel to the regional field. Many of the events in this cluster are located within the central portion of the impact crater (Figures 4a and 4c). This is notable because the central part of the crater is the region of most intense impact related faulting and fracturing [*Rondot*, 1994; *Lemieux et al.*, 2003], resulting in a variably oriented collection of potential failure planes. Results of the models also suggest that the interior of the crater is a region of reduced rift fault slip (Figure 10). The large availability of failure planes as well as the reduced rift fault slip suggest that focal mechanisms in this region would be among those least biased by the geometry of the St. Lawrence rift, and thus provide the best local stress field estimates.

[39] The large structural geometric bias in focal mechanisms in the St. Lawrence valley lies in marked contrast to many stress inversion results from California and Japan, which are typically consistent with borehole derived stress estimates [*Townend and Zoback*, 2001, 2006]. The contrast, however, may be due to a fundamental difference between the seismicity of tectonically active regions versus continental interiors. Since a single stress tensor is capable of reactivating faults in a variety of orientations [*McKenzie*, 1969], stress inversion techniques generally rely on sampling events from many variably oriented structures in a small geometric area to constrain a single stress tensor compatible with all derived slip directions [e.g., *Gephart and Forsyth*, 1984; *Arnold and Townend*, 2007]. Tectonically active areas surrounding plate boundaries are characterized by broad deformation at relatively high strain rates; consequently the conditions necessary for stress inversion are easily met and cover large areas. The seismically active faults are also typically geologically young features which formed in the current tectonic regime, and therefore, would be expected to be favorably oriented for reactivation and produce good stress inversions. The conditions in intraplate seismic zones, however, are considerably different. Structures in continental interiors are characterized by significantly lower strain rates than those in tectonically active areas. Inevitably most intraplate regions produce an inadequate number of events to carry out a stress inversion. The few areas where there are sufficient seismic events are often associated with prominent preexisting weak structure (e.g., a rift zone or aulacogen) which formed in a different tectonic regime than what exists today. Under these conditions it is possible that the most prominent structures (i.e., the St. Lawrence rift) are poorly oriented for reactivation, although they may be the largest source of weakness.

[40] The discrepancy between the focal mechanisms from the rift faults and the regional stress orientation is similar in many respects to plate boundary-related mechanisms in tectonically active areas. Plate boundaries, as opposed to the broad deformation zone around them, are characterized by preferred orientations of faults with low frictional strength, which can be reactivated under very poorly oriented stress conditions. The archetypal example of this is the plate boundary strike-slip San Andreas fault in the San Francisco Bay area California. Here the orientation of $S_H$ in the surrounding crust, as inferred from both borehole measurements and focal mechanism stress inversion is nearly perpendicular to the fault [e.g., *Zoback et al.*, 1987; *Townend*, 2006]. The influence of the plate boundary geometry dominates the overall kinematics, such that the focal mechanisms from slip along the fault may give misleading results for use in stress estimates. Consequently, focal mechanisms which are thought to be possible plate boundary events are flagged as such in the World Stress Map database, and are omitted by default from stress maps [*Barth et al.*, 2008]. Off the plate boundary, faults are more varied in orientations and stress inversion results are generally consistent with borehole data [*Townend and Zoback*, 2001]. If similar behavior affects the St. Lawrence, it implies that mechanisms within the rift zones with nodal planes consistent with slip along the rift faults should be treated as suspect.

[41] The apparent inherent weakness of the St. Lawrence rift raises the question as to whether similar behavior should

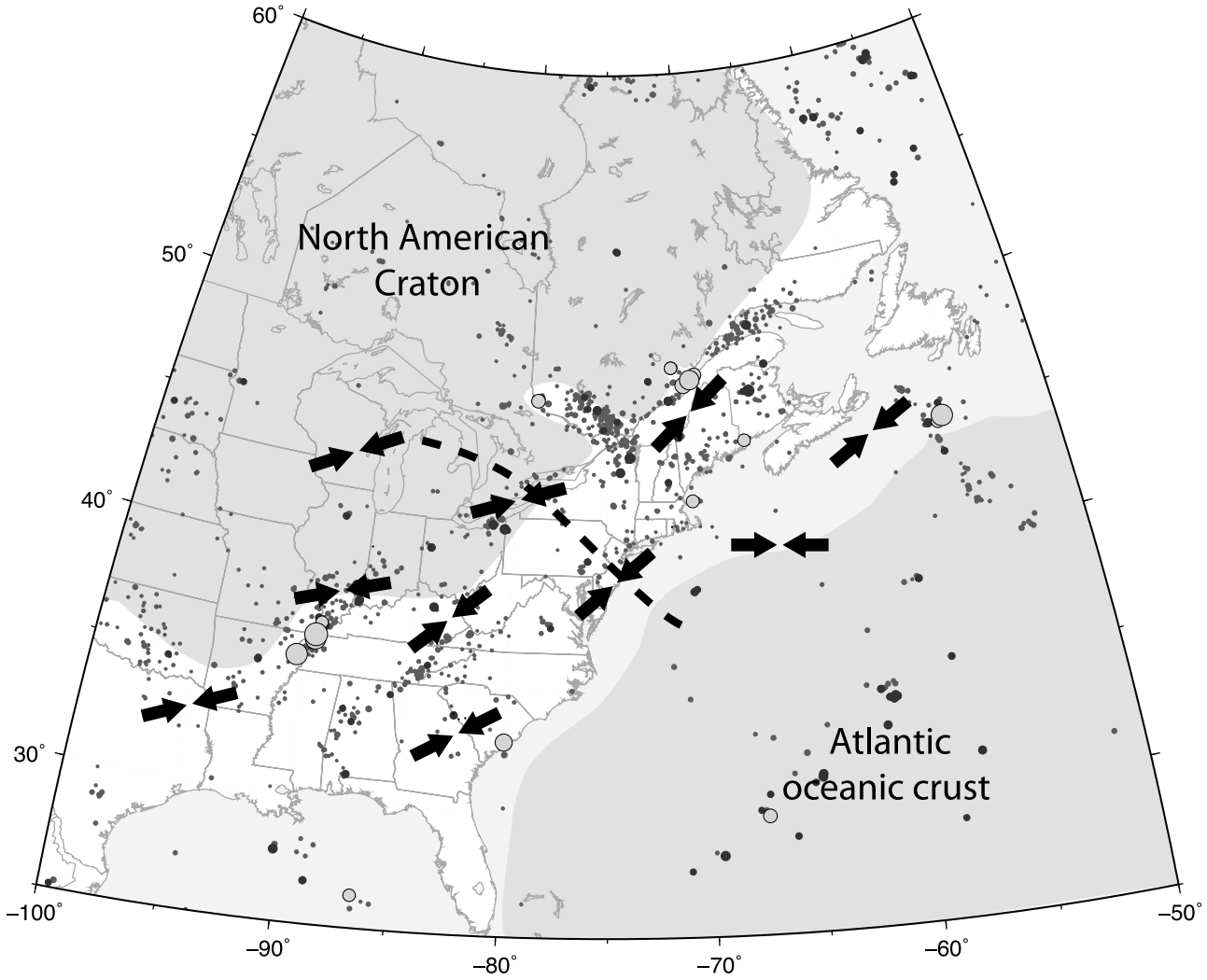


**Figure 12.** Seismicity and simplified stress map of eastern North America. Background seismicity since 1973 is shown by dark grey ($M \geq 3$) and black ($M \geq 4.5$) circles. Historical large earthquakes (mostly $M \geq 6.0$) are shown by large grey circles. Grey shaded area indicates the low-seismicity regions of the North American craton and the Atlantic oceanic crust (modified from *Mazzotti* [2007]). Inverted arrows show a generalized variation of $S_H$ orientation based on data from the World Stress Map [*Heidbach et al.*, 2008]. Dashed line indicates the approximate transition in earthquake focal mechanism style from predominately thrust in the northeast to predominately strike slip to the southwest (based on the focal mechanism compilation of *Mazzotti and Townend* [2010]). Seismicity data are from the Geological Survey of Canada and U.S. Geological Survey catalogs; historic Canadian events are from *Lamontagne et al.* [2007].

be expected in other intraplate seismic zones. *Johnston* [1993] noted that there is a global correlation between intraplate seismicity and regions of crustal extension, with about two thirds of events occurring within them. This correlation is particularly evident in eastern North America where most of the $M > 6$ events have occurred within the Atlantic and Iapetan rift basins, rifted margin, and aulacogens [*Mazzotti*, 2007]. This correlation is also reflected in the background seismicity (Figure 1). However, unlike the St. Lawrence rift, most events along these other rift structures produce focal mechanisms broadly consistent with the regional stress field [*Zoback*, 1992b; *Du et al.*, 2003]. This consistency may be partially due to the arrangement of structures relative to the stress field. In eastern Canada, for example, besides the CSZ and Lower St. Lawrence which lie along the NE trending St. Lawrence rift, many of the seismic zones lie along NW-SE oriented structures, such as the Ottawa and Saguenay grabens (Figure 1). These structures are approximately perpendicular to the regional orientation of $S_H$ and therefore are optimally oriented to reactivate in the thrust sense, which is prominent in eastern Canada. In the eastern United States paleotectonic rift structures are prominently oriented NE-SW, similar to that of the St. Lawrence. The transition south is also marked by some changes in the regional stress field, including a slight clockwise rotation in $S_H$ to ENE-WSW in the eastern central US, and perhaps more importantly a transition from prominently thrust regime in Canada to strike slip in the United States (Figure 12). The result is that the stress field is oriented at an acute angle to the major rift faults, which is more favorably oriented for reac-

tivation in a strike-slip sense. The implication is that the apparent consistency between the $S_H$ orientation and P axes may be due to a serendipitous arrangement of weak structures in the stress field that is optimally oriented for fault slip.

## 7. Conclusions

[42] The results of the 3-D stress models of the CSZ agree well with the main findings of the previously published 2-D models [*Baird et al.*, 2009]. Much of the background seismicity patterns can be explained by the intersection of weak faults of the St. Lawrence rift with the damage zone created by the Charlevoix impact. The weak faults modify the pattern of stress around the crater resulting in a stress concentration in the volume between the rift faults within and beneath the crater. In addition to matching broad patterns in seismicity, the 3-D models are able to explain subtle details in the seismicity distribution including the extension of background events to the NE of the crater. The best matching patterns from the models occur when the applied stress field is oriented parallel to the regional field as inferred from borehole breakout data. This suggests that there is no significant local source of stress driving the seismicity; however, to achieve the best calibration, the modeling results require that the rift faults be inherently weak.

[43] Modeled slip distribution along the main rift faults in response to boundary displacements shows that while slip is distributed throughout the rift, it is locally diminished inside the crater and locally enhanced just outside its boundaries. The area of enhanced slip agrees well with the location of large earthquakes just outside the boundary of the crater. Analysis of the slip vectors of events on the rift fault reveals an inferred P axis strongly oblique to the regional orientation of $S_H$, and broadly matching the style of large event focal mechanisms.

[44] The models suggest that the inherent weakness of the St. Lawrence rift may be producing a systematic rotation of focal mechanism P axes relative to the surrounding orientation of $S_H$. The effect appears to have a greater influence on large events, which preferentially occur along the regional faults, suggesting that small events may provide better indications of the true local state of stress. It is speculated that similar behavior may be expected in other seismically active intraplate rift zones, highlighting a potential caveat for the use of focal mechanisms for stress field estimation in intraplate settings in which seismicity is dominated by large structural features.

[45] **Acknowledgments.** We thank Stephane Mazzotti for providing us with an early version of his manuscript as well as a compilation of focal mechanism parameters. We are grateful for the helpful comments and suggestions of two anonymous reviewers and the Editor Tom Parsons. Financial support for this work was provided by the Ontario Research and Development Challenge Fund, Natural Sciences and Engineering Research Council of Canada Discovery Grants to Steve McKinnon and Laurent Godin and by an Ontario Graduate Scholarship in Science and Technology to Alan Baird.

## References

Adams, J., and G. Atkinson (2003), Development of seismic hazard maps for the proposed 2005 edition of the National Building Code of Canada, *Can. J. Civ. Eng.*, *30*(2), 255–271, doi:10.1139/l02-070.

Adams, J., and P. Basham (1991), The seismicity and seismotectonics of eastern Canada, in *Neotectonics of North America*, edited by D. B. Slemmons et al., pp. 261–275, *Geol. Soc. of Am.*, Boulder, Colo.

Adams, J., and J. S. Bell (1991), Crustal stresses in Canada, in *Neotectonics of North America*, edited by D. B. Slemmons et al., pp. 367–386, *Geol. Soc. of Am.*, Boulder, Colo.

Adams, J., and S. Halchuk (2003), Fourth generation seismic hazard maps of Canada: Values for over 650 Canadian localities intended for the 2005 National Building Code of Canada, *Geol. Surv. Can. Open File*, *4459*, 155 pp.

Anglin, F. M. (1984), Seismicity and faulting in the Charlevoix zone of the St. Lawrence valley, *Bull. Seismol. Soc. Am.*, *74*(2), 595–603.

Arnold, R., and J. Townend (2007), A Bayesian approach to estimating tectonic stress from seismological data, *Geophys. J. Int.*, *170*(3), 1336–1356, doi:10.1111/j.1365-246X.2007.03485.x.

Baird, A. F., S. D. McKinnon, and L. Godin (2009), Stress channelling and partitioning of seismicity in the Charlevoix seismic zone, Québec, Canada, *Geophys. J. Int.*, *179*(1), 559–568, doi:10.1111/j.1365-246X.2009.04275.x.

Barth, A., J. Reinecker, and O. Heidbach (2008), World Stress Map project guidelines: Stress derivation from earthquake focal mechanisms, GFZ-Potsdam, Potsdam, Germany. (Available at http://dc-app3-14.gfz-potsdam.de/pub/guidelines/WSM_analysis_guideline_focal_mechanisms.pdf)

Bent, A. L. (1992), A re-examination of the 1925 Charlevoix, Québec, earthquake, *Bull. Seismol. Soc. Am.*, *82*(5), 2097–2113.

Du, W.-X., W.-Y. Kim, and L. R. Sykes (2003), Earthquake source parameters and state of stress for the northeastern United States and southeastern Canada from analysis of regional seismograms, *Bull. Seismol. Soc. Am.*, *93*(4), 1633–1648, doi:10.1785/0120020217.

Fossum, A. F. (1985), Effective elastic properties for a randomly jointed rock mass, *Int. J. Rock Mech. Min. Sci. Geomech. Abstr.*, *22*(6), 467–470.

Gephart, J. W., and D. W. Forsyth (1984), An improved method for determining the regional stress tensor using earthquake focal mechanism data; application to the San Fernando earthquake sequence, *J. Geophys. Res.*, *89*(B11), 9305–9320, doi:10.1029/JB089iB11p09305.

Grana, J. P., and R. M. Richardson (1996), Tectonic stress within the New Madrid seismic zone, *J. Geophys. Res.*, *101*(B3), 5445–5458, doi:10.1029/95JB03255.

Hasegawa, H. S., and R. J. Wetmiller (1980), The Charlevoix earthquake of 19 August 1979 and its seismo-tectonic environment, *Earthquake Notes*, *51*(4), 23–37.

Hasegawa, H. S., J. Adams, and K. Yamazaki (1985), Upper crustal stresses and vertical stress migration in eastern Canada, *J. Geophys. Res.*, *90*(B5), 3637–3648, doi:10.1029/JB090iB05p03637.

Heidbach, O., M. Tingay, A. Barth, J. Reinecker, D. Kurfeß, and B. Müller (2008), The 2008 release of the World Stress Map, GFZ-Potsdam, Potsdam, Germany. (Available at http://dc-app3-14.gfz-potsdam.de/pub/release2008/release2008.html)

Itasca Consulting Group Inc (2005), FLAC3D (Fast Lagrangian Analysis of Continua in 3 Dimensions), Version 3.0, Minneapolis, Minn.

Johnston, A. C. (1993), Average stable continental earthquake source parameters based on constant stress drop scaling, *Seismol. Res. Lett.*, *64*, 261.

Kumarapeli, P. S. (1985), Vestiges of Iapetan rifting in the craton west of the northern Appalachians, *Geosci. Can.*, *12*(2), 54–59.

Lamontagne, M. (1999), Rheological and geological constraints on the earthquake distribution in the Charlevoix seismic zone, Québec, Canada [CD-ROM], *Geol. Surv. Can. Open File*, *D3778*.

Lamontagne, M., and G. Ranalli (1996), Thermal and rheological constraints on the earthquake depth distribution in the Charlevoix, Canada, intraplate seismic zone, *Tectonophysics*, *257*(1), 55–69, doi:10.1016/0040-1951(95)00120-4.

Lamontagne, M., S. Halchuk, J. F. Cassidy, and G. C. Rogers (2007), Significant Canadian earthquakes 1600–2006, *Geol. Surv. Can. Open File*, *5539*.

Leblanc, G., A. E. Stevens, R. J. Wetmiller, and R. DuBerger (1973), A micro-earthquake survey of the St. Lawrence valley near La Malbaie, Quebec, *Can. J. Earth Sci.*, *10*(1), 42–53.

Lemieux, Y., A. Tremblay, and D. Lavoie (2003), Structural analysis of supracrustal faults in the Charlevoix area, Quebec: Relation to impact cratering and the St-Laurent fault system, *Can. J. Earth Sci.*, *40*(2), 221–235, doi:10.1139/e02-046.

Mazzotti, S. (2007), Geodynamic models for earthquake studies in intraplate North America, in *Continental Intraplate Earthquakes: Science, Hazard, and Policy Issues*, edited by S. Stein and S. Mazzotti, *Spec. Pap. Geol. Soc. Am.*, *425*, 17–33, doi:10.1130/2007.2425(02).

Mazzotti, S., and J. Townend (2010), State of stress in central and eastern North American seismic zones, *Lithosphere*, *2*(2), 76–83, doi:10.1130/L65.1.

McKenzie, D. P. (1969), The relation between fault plane solutions for earthquakes and the directions of the principal stresses, *Bull. Seismol. Soc. Am.*, *59*(2), 591–601.

Richardson, R. M., and L. M. Reding (1991), North American plate dynamics, *J. Geophys. Res.*, *96*(B7), 12,201–12,223, doi:10.1029/91JB00958.

Rivers, T. (1997), Lithotectonic elements of the Grenville Province: review and tectonic implications, *Precambrian Res.*, *86*(3-4), 117–154, doi:10.1016/S0301-9268(97)00038-7.

Rondot, J. (1971), Impactite of the Charlevoix structure, Quebec, Canada, *J. Geophys. Res.*, *76*(23), 5414–5423, doi:10.1029/JB076i023p05414.

Rondot, J. (1994), Recognition of eroded astroblemes, *Earth Sci. Rev.*, *35*(4), 331–365, doi:10.1016/0012-8252(94)90001-9.

Solomon, S. C., and E. D. Duxbury (1987), A test of the longevity of impact-induced faults as preferred sites for later tectonic activity, *Proc. 17th Lunar Planet. Sci. Conf., Part 2*, *J. Geophys. Res.*, *92*(B4), E759–E768, doi:10.1029/JB092iB04p0E759.

Somerville, P. G., J. P. McLaren, C. K. Saikia, and D. V. Helmberger (1990), The 25 November 1988 Saguenay, Quebec, earthquake: Source parameters and the attenuation of strong ground motion, *Bull. Seismol. Soc. Am.*, *80*(5), 1118–1143.

Stein, S. (2007), Approaches to continental intraplate earthquake issues, in *Continental Intraplate Earthquakes: Science, Hazard, and Policy Issues*, edited by S. Stein and S. Mazzotti, *Spec. Pap. Geol. Soc. Am.*, *425*, 1–16, doi:10.1130/2007.2425(01).

St-Julien, P., and C. Hubert (1975), Evolution of the Taconian orogen in the Quebec Appalachians, *Am. J. Sci.*, *275-A*, 337–362.

Sykes, L. R. (1978), Intraplate seismicity, reactivation of preexisting zones of weakness, alkaline magmatism, and other tectonism postdating continental fragmentation, *Rev. Geophys. Space Phys.*, *16*(4), 621–688, doi:10.1029/RG016i004p00621.

Townend, J. (2006), What do faults feel? Observational constraints on the stresses acting on seismogenic faults, in *Earthquakes: Radiated Energy and the Physics of Faulting*, *Geophys. Monogr. Ser.*, vol. 170, edited by R. Abercrombie et al., pp. 313–327, doi:10.1029/170GM31, AGU, Washington, D. C.

Townend, J., and M. D. Zoback (2001), Implications of earthquake focal mechanisms for the frictional strength of the San Andreas fault system, in *The Nature and Tectonic Significance of Fault Zone Weakening*, edited by R. E. Holdsworth et al., *Geol. Soc. Spec. Publ.*, *186*, 13–21, doi:10.1144/GSL.SP.2001.186.01.02.

Townend, J., and M. D. Zoback (2006), Stress, strain, and mountain building in central Japan, *J. Geophys. Res.*, *111*, B03411, doi:10.1029/2005JB003759.

Tremblay, A., B. Long, and M. Massé (2003), Supracrustal faults of the St. Lawrence rift system, Québec: kinematics and geometry as revealed by field mapping and marine seismic reflection data, *Tectonophysics*, *369*(3-4), 231–252, doi:10.1016/S0040-1951(03)00227-0.

Zoback, M. D., and M. L. Zoback (1991), Tectonic stress field of North America and relative plate motions, in *Neotectonics of North America*, edited by D. B. Slemmons, E. R. Engdahl, M. D. Zoback, and D. D. Blackwell, pp. 339–366, Geol. Soc. of Am., Boulder, Colo.

Zoback, M. D., et al. (1987), New evidence on the state of stress of the San Andreas fault system, *Science*, *238*(4830), 1105–1111, doi:10.1126/science.238.4830.1105.

Zoback, M. D., et al. (1993), Upper-crustal strength inferred from stress measurements to 6 km depth in the KTB borehole, *Nature*, *365*(6447), 633–635, doi:10.1038/365633a0.

Zoback, M. L. (1992a), First- and second-order patterns of stress in the lithosphere: The World Stress Map Project, *J. Geophys. Res.*, *97*(B8), 11,703–11,728, doi:10.1029/92JB00132.

Zoback, M. L. (1992b), Stress field constraints on intraplate seismicity in eastern North America, *J. Geophys. Res.*, *97*(B8), 11,761–11,782, doi:10.1029/92JB00221.

Zoback, M. L., and R. M. Richardson (1996), Stress perturbation associated with the Amazonas and other ancient continental rifts, *J. Geophys. Res.*, *101*(B3), 5459–5475, doi:10.1029/95JB03256.

A. F. Baird, L. Godin, and S. D. McKinnon, Department of Geological Sciences and Geological Engineering, Queen's University, Kingston, ON K7L 3N6, Canada. (baird@geol.queensu.ca; godin@geol.queensu.ca; sm@mine.queensu.ca)